WILEY-VCH

DOI: 10.1002/((please add manuscript number))
Article type: Communication

Rust-Mediated Continuous Assembly of Metal-Phenolic Networks

*Md. Arifur Rahim, Mattias Björnmalm, Nadja Bertleff-Zieschang, Quinn Besford, Srinivas Mettu, Tomoya Suma, Matthew Faria, and Frank Caruso**

Dr. M. A. Rahim, Dr. M. Björnmalm, Dr. N. Bertleff-Zieschang, Dr. Q. Besford, T. Suma, M. Faria, Prof. F. Caruso
ARC Centre of Excellence in Convergent Bio-Nano Science and Technology, and the Department of Chemical and Biomolecular Engineering, the University of Melbourne, Parkville, Victoria 3010, Australia

Dr. S. Mettu
Department of Chemical and Biomolecular Engineering, the University of Melbourne, Parkville, Victoria 3010, Australia

Keywords: rust, etching, chelates, self-assembly, metal-phenolic networks

Innovative synthetic methods in materials science expand the limits of functional systems by generating new insights and refining existing knowledge, and can often lead to new materials or properties difficult to obtain otherwise.[1-7] These developments can significantly impact the technological transformation and future directions of research fields.[2,4,8] Examples include advances in synthetic strategies in the fields of: (1) metal-organic frameworks, e.g., from solvothermal to spray drying methods, and (2) surface engineering through layer-by-layer assembly, e.g., from immersion assembly to electrophoretic assembly methods.[2,8,9]

Recently, we demonstrated a one-step, interfacial assembly method for hybrid film formation utilizing metal-phenolic coordination chemistry that results in metal-phenolic networks (MPNs).[10] These amorphous, surface-confined MPN films have potential for a range of applications, including drug delivery, bio-imaging, separations, and catalysis.[10-13] This research field is still in its infancy and previous studies have mainly focused on designing MPN systems with different metal-phenolic combinations or exploring their potential applications. In contrast, less attention has been given to the development of new synthetic strategies.[14-18] The original synthetic method for MPN formation—mixing solutions of phenolic ligands and metal ions in the presence of solid substrates—is inherently limited by the apparent discrete nature of the self-assembly process. Film growth occurs rapidly (<1 min) and film thickness is of the order of 10 nm, irrespective of the type of metal, ligand, or assembly conditions used.[10-12] Hence, novel synthetic approaches that enable the continuous assembly of MPNs—that are fundamentally different to discrete assembly—may afford MPN systems with processing flexibility, tunable properties, and expand our current understanding of such metal-ligand molecular interactions.

Herein, we introduce a new strategy using rusted iron objects (e.g., rusted nails) as solid-state iron sources for the fabrication of MPNs. Using this strategy, we demonstrate that the assembly process for MPNs can be modulated from discrete to continuous. The reaction between gallic acid (GA; a naturally abundant phenolic compound) solution and a rusted iron

nail generates chelate complexes in solution (via etching of the rust layer) which self-assemble and grow stable networks on particulate substrates dispersed in the system. In contrast to previous studies, this continuous assembly process enables the film thickness to be controlled as a function of time. This study provides insight into the interfacial chemistry of metal-phenolic complexes while also demonstrating a new concept in the emerging research area at the interface of materials science and green chemistry: the preparation of advanced materials with tailored properties using waste products (e.g., rusted objects).[19]

The experimental setup used in this study is presented in **Figure 1**a-i. A rusted nail (Figure 1a and Figure S1 in the Supporting Information) was immersed in GA (Figure 1b) solution containing particulate substrates (polystyrene, PS), as shown in Figure 1c-e. The GA/PS dispersion turned increasingly dark (blue-black) over time (Figure 1f-i), suggesting progressive etching of iron ions from the rust layer via chelation by GA. The chelate complexes thus generated were able to self-assemble and form MPN films on the solid substrates (see below). Note that “rust” is a commonly used term in corrosion science and is characterized by the presence of iron(III) oxyhydroxide phases (e.g., lepidocrocite and akaganeite).[20-22] We use “rust” to refer to these types of phases and to distinguish from “iron oxide” due to the specificity of the phenolic etching toward the oxyhydroxide phases of rust (see below).

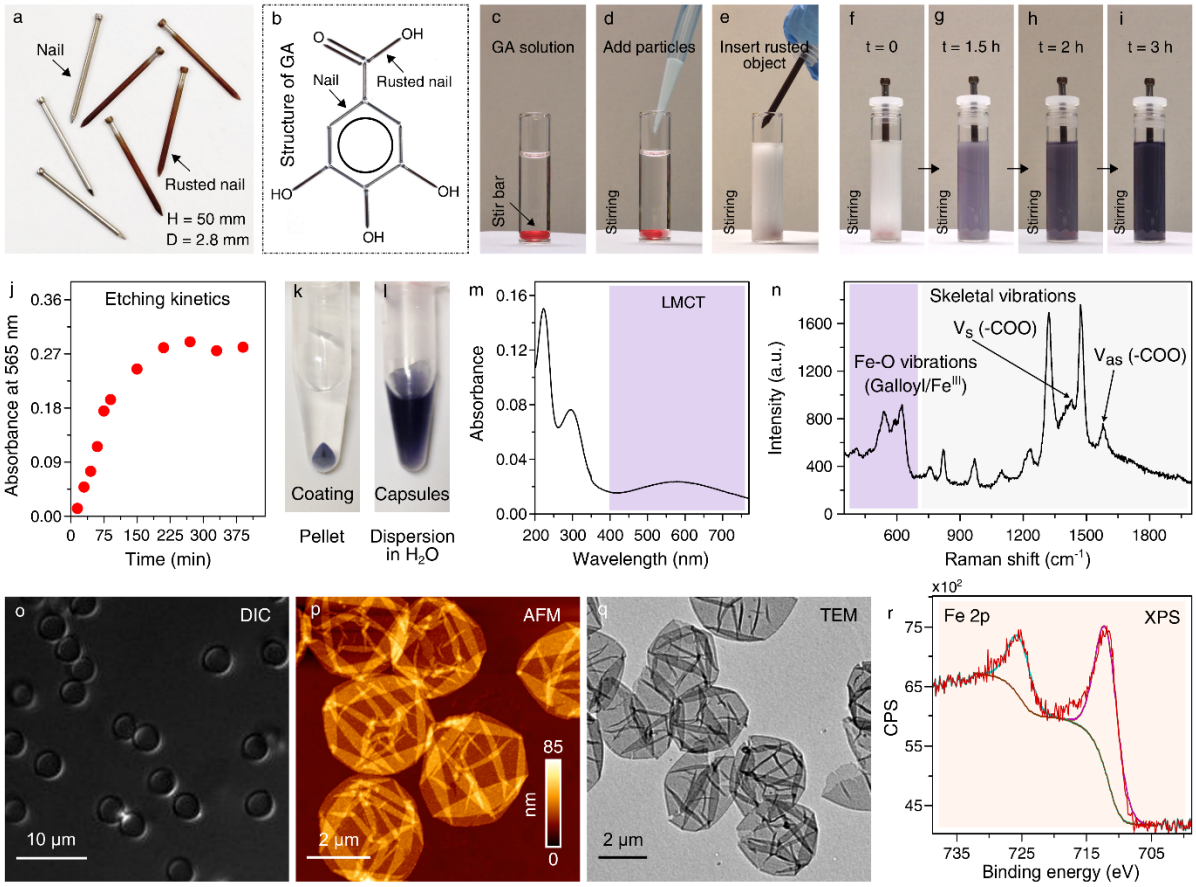

Figure 1. a, Photographs of randomly arranged rusted and non-rusted iron nails. **b**, Structural representation of GA by arranging rusted and non-rusted iron nails. **c-i**, Photographs of the continuous assembly process in sequence. **j**, Etching kinetics as monitored by UV-Vis absorption spectroscopy (LMCT band) over time. Photographs showing the coating on particulate PS substrates (**k**) after washing and pelleting through centrifugation, and freestanding capsules (**l**) (concentrated dispersion) obtained after substrate removal and redispersion in water. **m**, UV–Vis absorption spectrum of GA/R-Fe^{III} system showing the LMCT band. **n**, RR spectrum showing the different coordination modes in the GA/R-Fe^{III} system. **o**, DIC image of GA/R-Fe^{III} capsules showing the monodisperse capsules. Surface morphologies of the GA/R-Fe^{III} capsules as observed by AFM (**p**) and TEM (**q**). **r**, XPS core-level spectrum showing the presence of Fe^{III} in GA/R-Fe^{III} capsules.

The etching process (without adding the solid substrates) of a rusted nail was first monitored by UV-Vis absorption spectroscopy. The characteristic ligand-to-metal charge transfer (LMCT) band of GA/iron(III) (GA/Fe^{III}) complexes appeared at ~565 nm,[11,23] the intensity of which continued to increase as a function of time (Figure S2) and was observed to saturate around 4 h (Figure 1j). Based on this observation, we investigated the continuous assembly process for film formation within this time range. X-ray photoelectron spectroscopy (XPS) analysis on the rust (Figure S3) revealed an oxidation state of III for Fe[11] and no other metals were detected. X-ray diffraction (XRD) (Figure S4) performed on the rust detected a crystalline phase of β-FeO(OH) (akaganeite).[24] These results suggest the etching process was initiated by GA coordinating Fe^{III} ions from the rust layer. Etching tests performed for pure iron and iron(III) oxide (Fe_2O_3) in GA solution were not successful (Figure S5), suggesting the specific nature of the etching process toward iron(III) oxyhydroxide phases present in rust.

The films and capsules obtained after 1.5 or 2 h of immersion of the rusted nail in the GA/PS dispersion were extensively characterized. We denote these films as GA/R-Fe^{III} (where R-Fe^{III} stands for iron(III) ions sourced from rust). The GA/R-Fe^{III} coatings can be visualized by the dark coloration of the PS particles and through the formation of free-standing capsules after dissolving the template PS particles (Figure 1k,l). UV-Vis absorption spectra of the GA/R-Fe^{III} system (Figure 1m) showed the LMCT band at ~565 nm, suggesting a bis-type coordination mode dominant in the film structures.[11,23] The metal-ligand interactions in GA/R-Fe^{III} films were further probed by resonance Raman (RR) spectroscopy (Figure 1n). RR spectrum revealed bands in the high frequency region around 1470, 1320, and 1230 cm^{-1}, which can be attributed to the skeletal modes of substituted benzene ring.[11,25,26] Bands in the low frequency region of 650–400 cm^{-1} can be attributed to the Fe-O vibration (ν_{Fe-O}) due to galloyl-Fe^{III} interactions.[11,25] In addition, bands at 1578 and 1430 cm^{-1} arising from asymmetric and symmetric stretching of carboxylate (-COO) group (ν_{as}, and ν_s, respectively), can be assigned to (-COO)/Fe^{III} interactions.[27] The difference (Δ_{s-as}) between

these two bands (ν_{as} and ν_s) is 148 cm^{-1}, suggesting a type-III bridging mode (Figure S6) of (-COO)/Fe^{III}.[25,27] XRD analysis (Figure S7) confirmed the amorphous phase of the GA/R-Fe^{III} system that is indicative of a self-assembly process via kinetic trapping, as described previously.[11]

Differential interference contrast (DIC) microscopy images of the GA/R-Fe^{III} system showed stable and monodisperse capsules (Figure 1o). The dried GA/R-Fe^{III} capsules (1.5 h) revealed surface morphologies (folds and creases) typical of collapsed capsules (Figure 1p) as investigated by atomic force microscopy (AFM).[10] Analyzing the AFM height profiles, the shell thickness of the capsules was found to be ~5 nm (Figure S8) with a root-mean-square (rms) roughness value of ~0.8 nm. This is the thinnest of all MPN capsule systems reported so far.[10-12,18] Transmission electron microscopy (TEM) images of the capsules showed similar surface features as observed by AFM (Figure 1q). XPS data for GA/R-Fe^{III} capsules showed the Fe 2p3/2 signal at ~712 eV with a 2p peak separation of ~14 eV (Figure 1r). This result confirmed the higher oxidation state (III) of iron as the dominant species in the films.[11] Based on the results above, it can be suggested that the structural compositions of GA/R-Fe^{III} (a possible network structure of GA/R-Fe^{III} is shown in **Scheme 1**) and GA/Fe^{III} (solution based, no solid-state iron source)[11] are qualitatively similar except that the latter contains both mono and polymeric Fe species in its coordinated network structure, as discussed below.

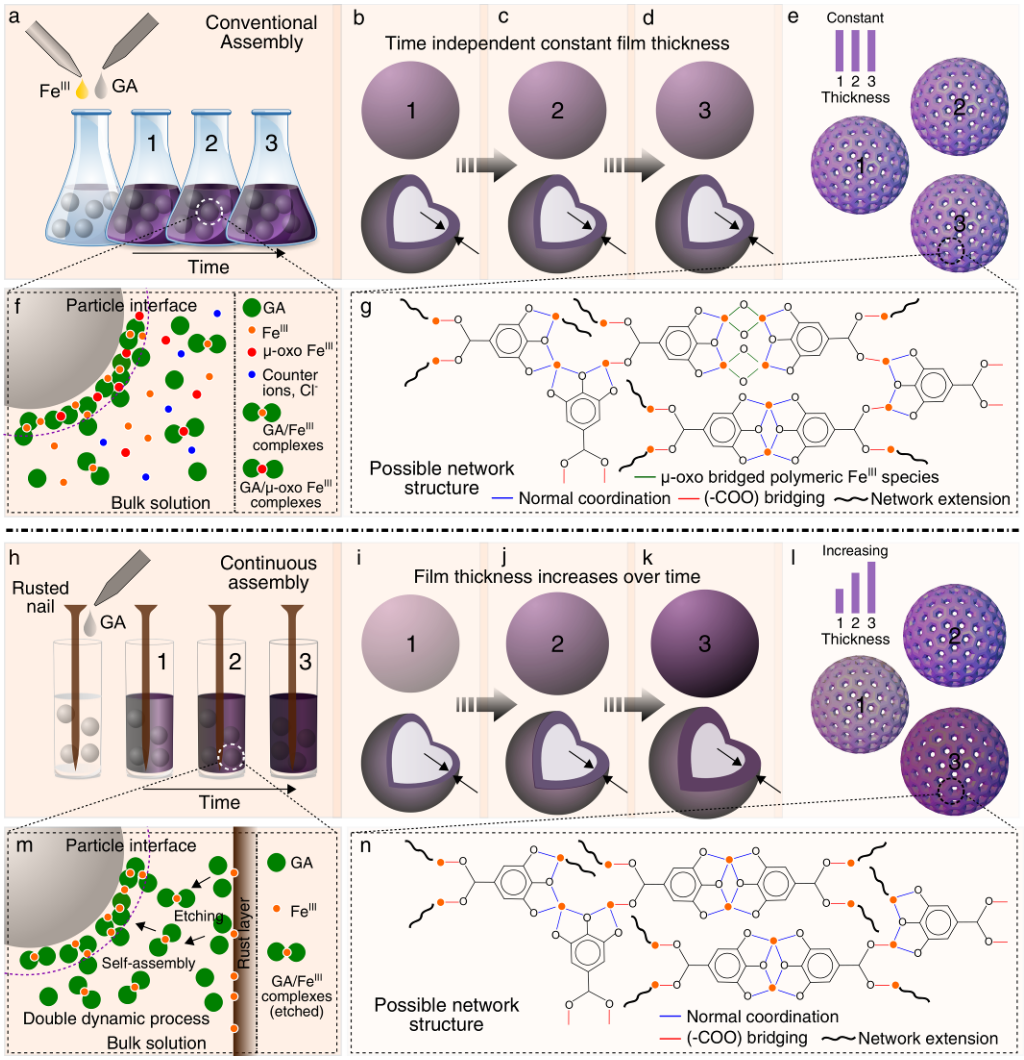

Scheme 1. Comparison of the conventional (iron source in solution) and continuous (solid-state iron source) assembly processes. Conventional assembly process (**a-e**), various complex species at the interface and in the bulk (**f**), and the possible molecular structure of the resulting networks (**g**). Continuous assembly process (**h-l**), various complex species at the interface and in the bulk (**m**), and the possible molecular structure of the resulting networks (**n**). Note that the apparent porous structures in the illustrations of the capsules (e,l) refer to the coordination networks (connected hexagons) at the molecular level.

The current strategy possesses several fundamental differences when compared to the conventional (solution-based) MPN synthesis[10,11] (Scheme 1), such as: (1) introduction of solid-state reactants (rusted iron objects/nails) instead of iron salt solutions (Scheme 1a,h); (2)

the absence of counter ions from metal salts (e.g., Cl^- from $FeCl_3.6H_2O$) (Scheme 1f,m);[10,11] (3) the absence of polymeric (i.e., μ-oxo bridged) Fe species (due to hydrolysis of iron salts in aqueous media) in solution (Scheme 1f,m) and the resulting networks (compare Scheme 1g,n, μ-oxo bridging is indicated by green bonds),[28,29] since Fe ions from rust (note that rust is insoluble in water) are etched (transferred into solution) through complexation with GA; (4) the presence of a time-dependent double-dynamic process: i.e., etching and self-assembly (Scheme 1b-e,i-l); (5) the continuous nature of the self-assembly process (Scheme 1a-e,h-l) as opposed to the discrete nature of that in the solution-based self-assembly process; (6) time-dependent control over the film thickness (Scheme 1b-e,i-l); and (7) utilization of waste corrosion products as reactants.

We hypothesize that the continuous generation of the complexes (GA/Fe^{III})—enabled by the rust source—and the continuous supply of these complexes to the template interface is essential for modulating the fundamental nature of the assembly (i.e., from discrete to continuous). In our current approach, this is achieved by the continuous etching of Fe from the rust layer by GA. Moreover, the low ionic strength (considering the counter ions and various ionic species present in the conventional synthesis, compare panels f and m in Scheme 1) of this system may also facilitate the observed continuous growth of the films. However, additional studies are required to fully elucidate the underlying mechanism of the assembly process.

The continuous nature of the self-assembly process presented here is evident from the time dependent thickness growth of the MPN films. As presented in Figures 2a-e, the GA/R-Fe^{III} capsule shells were found to grow thicker over time. Capsules with a shell thickness ranging from ~5 nm (**Figure 2**a; capsules with thicknesses of <5 nm were not stable during template removal) to ~70 nm (Figures 2e and S9) could be obtained with the different conditions investigated herein (see Supporting Information). This can be compared to the ~10 nm that is obtained using the conventional (i.e., no solid-state iron source) assembly

method.[10] To further investigate the effect of reaction time on film thickness at shorter time scales, we took samples between 1.5 and 4 h with a frequency of 15 min for first 3 h (Figure 1f-i). As evidenced by Figures 2a-d and S10, the film thickness in this case could be tuned from ~5 to ~31 nm with a growth rate of roughly 0.16 nm per min. The roughness differences among the GA/R-Fe^{III} capsules with different thicknesses were negligible (all showed rms roughness values around ~0.8-1.3 nm, as measured by AFM). In agreement with the AFM analyses above, the color and LMCT bands of the capsules with increasing thicknesses intensified over time (Figure 2f).

We also investigated the disassembly and mechanical properties of the GA/R-Fe^{III} capsules with different thicknesses (approx. 10, 20, and 30 nm). Disassembly (in terms of film composition) of GA/R-Fe^{III} capsules dispersed in buffer solutions of pH 2 was monitored by following the decrease in the LMCT band intensity over time (Figure 2g). Differences in the disassembly kinetics were observed; for example, 50% disassembly occurred at 3, 5, and 7 min for the capsules with thicknesses of ~10, ~20, and ~30 nm, respectively (Figure 2g). In comparison, 50% disassembly of GA/Fe^{III} capsules (prepared via conventional solution-based assembly) with thickness of ~10 nm, occurred at 4 min at identical disassembly conditions as above (Figure S11).

The mechanical properties of the capsules were examined by colloidal-probe AFM force measurements. The stiffness of the capsules was observed to increase with increasing shell thickness, as shown by the representative force-deformation curves (Figure 2h):[30] the stiffnesses, determined from the slope of the curves, were found to be 56 ± 11, 166 ± 17, and 470 ± 59 mN m^{-1} for the ~10, ~20, and ~30 nm thick GA/R-Fe^{III} capsules, respectively (Figure S12). For the GA/R-Fe^{III} capsules of ~10 nm thickness, the Young's modulus (E_Y) was estimated to be 334 ± 63 MPa. This demonstrates that GA/R-Fe^{III} capsules, of similar

thickness, are considerably less stiff than the analogous GA/Fe^{III} capsules prepared using conventional (i.e., no solid-state iron source) assembly (E_Y of 620 ± 200 MPa).[11]

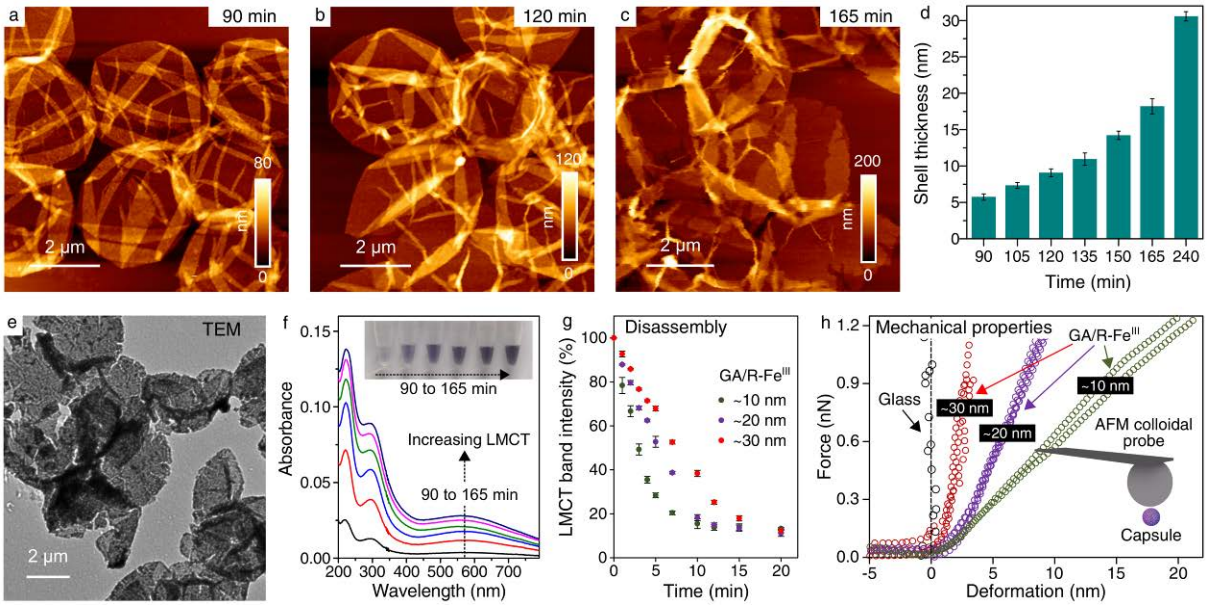

Figure 2. a-c, AFM topographies of the GA/R-Fe^{III} capsules with increasing thickness over time and the corresponding height analyses results (**d**). **e**, TEM micrograph of capsules with a shell thickness of around 70 nm (as determined using AFM). With the thicker MPN coatings, core removal became increasingly difficult, inducing large pores in the films and the collapsed, dried capsules appeared rougher under TEM. **f**, UV-Vis absorption spectra and photograph (inset) of the corresponding capsule dispersions in water. **g**, Disassembly profiles of the GA/R-Fe^{III} with increasing shell thickness. **h**, Representative force-deformation curves for the small deformation regime of GA/R-Fe^{III} capsules with increasing shell thickness (green, purple, and red circles for ~10, ~20, and ~30 nm, respectively). Glass (black circles) was included as a control.

Finally, we investigated the versatility and general applicability of the current strategy. First we replaced GA with another phenolic ligand, tannic acid (TA; a natural polyphenol, **Figure 3**a), and the TA/R-Fe^{III} system also successfully formed capsules (Figure 3b,c). UV-Vis absorption spectra for TA and TA/R-Fe^{III} capsule suspension (showing the LMCT band at

~570 nm) are shown in Figure 3d. Continuous assembly over time for this system is demonstrated in Figure S13. Next, iron objects rusted outdoor (due to natural weathering, Figure 3e) were collected and tested as solid-state iron sources for GA/R-Fe^{III} coating. Capsules could be assembled in each case as demonstrated by DIC imaging (Figures 3f and S14), and UV-Vis absorption (Figure S15). TEM and EDX analyses were used to further characterize the resulting GA/R-Fe^{III} capsules (Figures 3g,h and S16).

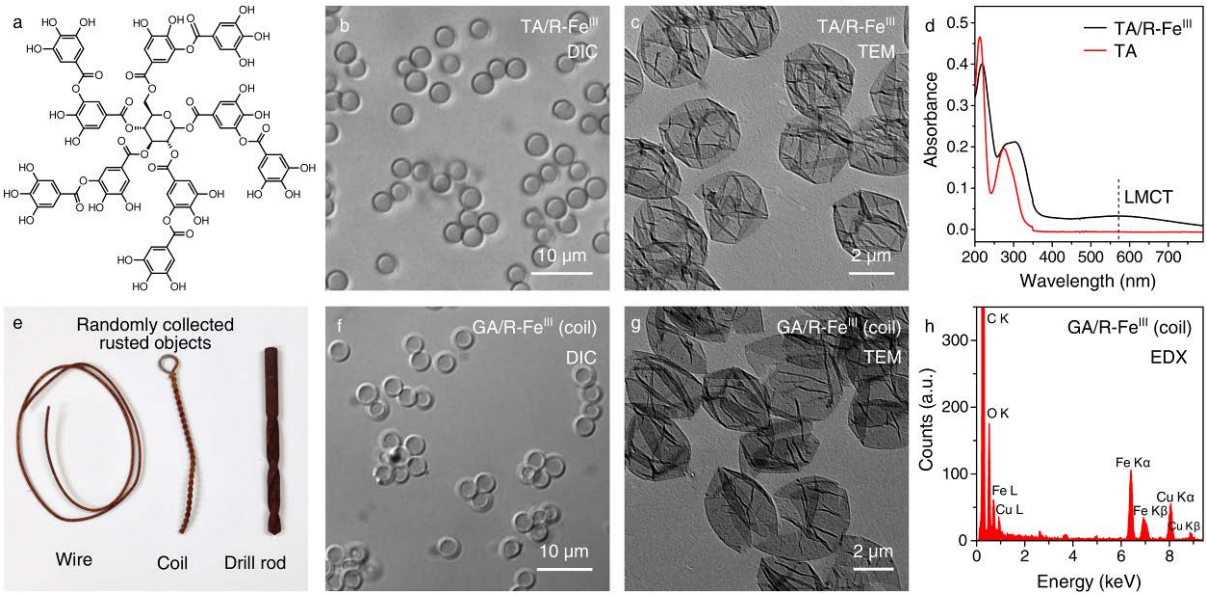

Figure 3. a, Structure of TA. DIC (**b**) and TEM (**c**) micrograph of TA/R-Fe^{III} capsules. **d**, UV–Vis absorption spectra of TA and the corresponding capsules showing the LMCT band. Collected iron objects rusted due to natural weathering (**e**) and their use as iron source for GA/R-Fe^{III} coating as shown by DIC (**f**), TEM (**g**), and EDX analysis (**h**).

In summary, we present a versatile approach to fabricate MPN films via a continuous assembly process using rust as a solid-state iron source. A unique feature of the current approach is that it enables for the thickness of MPN films to be controlled by adjusting the reaction time. In addition, this method may also improve the ease and scalability of the process, as continuous processes are typically preferred industrially.[2] The double dynamic process (etching of a solid-state iron source followed by interfacial self-assembly of metal-

phenolic complexes onto colloidal substrates) presented herein provides new insights into the nature of metal-phenolic interfacial assembly, while demonstrating a continuous method for the assembly of metal-phenolic films with controlled thickness.

Supporting Information

Supporting Information is available from the Wiley Online Library or from the author.

Acknowledgements

This research was supported by the Australian Research Council (ARC) under the Australian Laureate Fellowship (FL120100030) scheme, and the ARC Centre of Excellence in Convergent Bio-Nano Science and Technology (Project CE140100036). This work was performed in part at the Materials Characterisation and Fabrication Platform at the University of Melbourne and the Victorian Node of the Australian National Fabrication Facility.

Received: ((will be filled in by the editorial staff))

Revised: ((will be filled in by the editorial staff))

Published online: ((will be filled in by the editorial staff))

References

[1] J. H. Bang, K. S. Suslick, *Adv. Mater.* **2010**, *22*, 1039.

[2] J. J. Richardson, M. Björnmalm, F. Caruso, *Science* **2015**, *348*, aaa2491.

[3] I. Stassen, M. Styles, G. Grenci, H. V. Gorp, W. Vanderlinden, S. D. Feyter, P. Falcaro, D. D. Vos, P. Vereecken, R. Ameloot, *Nat. Mater.* **2016**, *15*, 304.

[4] N. Stock, S. Biswas, *Chem. Rev.* **2012**, *112*, 933.

[5] J. Zhou, B. Duan, Z. Fang, J. Song, C. Wang, P. B. Messersmith, H. Duan, *Adv. Mater.*, **2014**, *26*, 701.

[6] J. Zhou, P. Wang, C. Wang, Y. T. Goh, Z. Fang, P. B. Messersmith, H. Duan, *ACS Nano*, **2015**, *9*, 6951.

[7] E. Yamamoto, K. Kuroda, *Bull. Chem. Soc. Jpn.*, **2016**, *89*, 501.

[8] J. J. Richardson, J. Cui, M. Björnmalm, J. A. Braunger, H. Ejima, F. Caruso, *Chem. Rev.*, **2016**, *116*, 14828.

[9] A. Carné-Sánchez, I. Imaz, M. Cano-Sarabia, D. Maspoch, *Nat. Chem.* **2013**, *5*, 203.

[10] H. Ejima, J. J. Richardson, K. Liang, J. P. Best, M. P. van Koeverden, G. K. Such, J. Cui, F. Caruso, *Science* **2013**, *341*, 154.

[11] M. A. Rahim, K. Kempe, M. Müllner, H. Ejima, Y. Ju, M. P. van Koeverden, T. Suma, J. A. Braunger, M. G. Leeming, B. F. Abrahams, F. Caruso, *Chem. Mater.* **2015**, *27*, 5825.

[12] J. Guo, Y. Ping, H. Ejima, K. Alt, M. Meissner, J. J. Richardson, Y. Yan, K. Peter, D. von Elverfeldt, C. E. Hagemeyer, F. Caruso, *Angew. Chem. Int. Ed.* **2014**, *53*, 5546.

[13] Y. Ju, Q. Dai, J. Cui, Y. Dai, T. Suma, J. J. Richardson, F. Caruso, *ACS Appl. Mater. Interfaces* **2016**, *8*, 22914.

[14] P. Han, J. Shi, T. Nie, S. Zhang, X. Wang, P. Yang, H. Wu, Z. Jiang, *ACS Appl. Mater. Interfaces* **2016**, *8*, 8076.

[15] H. Liang, J. Li, Y. He, W. Xu, S. Liu, Y. Li, Y. Chen, B. Li, *ACS Biomater. Sci. Eng.* **2016**, *2*, 317.

[16] H. Ejima, J. J. Richardson, F. Caruso, *Polym. J.* **2014**, *46*, 452.

[17] L. Yang, L. Han, J. Ren, H. Wei, L. Jia, *Colloids Surf., A* **2015**, *484*, 197.

[18] M. Björnmalm, J. Cui, N. Bertleff-Zieschang, D. Song, M. Faria, M. A. Rahim, F. Caruso, *Chem. Mater.* **2017**, *29*, 289.

[19] D. Mhamane, H.-K. Kim, V. Aravindan, K. C. Roh, M. Srinivasan, K.-B. Kim, *Green Chem.* **2016**, *18*, 1395.

[20] Y. Zou, J. Wang, Y. Y. Zheng, *Corros. Sci.* **2011**, *53*, 208.

[21] Y. Zhao, H. Ren, H. Dai, W. Jin, *Corros. Sci.* **2011**, *53*, 1646.

[22] A. Collazo, X. R. Nóvoa, C. Pérez, B. Puga, *Electrochim. Acta* **2010**, *55*, 6156.

[23] M. J. Sever, J. J. Wilker, *Dalton Trans.* **2004**, 1061.

[24] A. Collazo, X. R. Nóvoa, C. Pérez, B. Puga, *Electrochim. Acta* **2008**, *53*, 7565.

[25] A. Ponce, L. B. Brostoff, S. K. Gibbons, P. Zavalij, C. Viragh, J. Hooper, S. Alnemrat, K. J. Gaskell, B. Eichhorn, *Anal. Chem.* **2016**, *88*, 5152.

[26] A. S. Lee, P. J. Mahon, D. C. Creagh, *Vib. Spectrosc.* **2006**, *41*, 170.

[27] G. B. Deacon, R. J. Phillips, *Coord. Chem. Rev.* **1980**, *33*, 227.

[28] S. W. Taylor, D. B. Chase, M. H. Emptage, M. J. Nelson, J. H. Waite, *Inorg. Chem.* **1996**, *35*, 7572.

[29] L. Lopes, J. de Laat, B. Legube, *Inorg. Chem.* **2002**, *41*, 2505.

[30] A. Fery, R. Weinkamer, *Polymer* **2007**, *48*, 7221.

Table of Contents

Don’t throw away your rusted objects! Rust can do wonders. A continuous assembly approach for the fabrication of metal-phenolic networks (MPNs) with tailored thicknesses using rusted objects as solid-state iron sources is reported. Using this strategy, it is demonstrated that the assembly process for MPNs can be modulated from discrete to continuous.

Keywords: rust, etching, chelates, self-assembly, metal-phenolic networks

M. A. Rahim, M. Björnmalm, N. Bertleff-Zieschang, Q. Besford, S. Mettu, T. Suma, M. Faria, F. Caruso

Rust-Mediated Continuous Assembly of Metal-Phenolic Networks

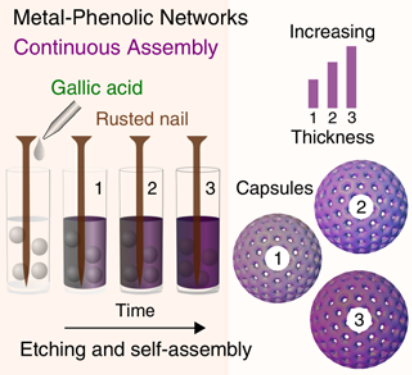

Copyright WILEY-VCH Verlag GmbH & Co. KGaA, 69469 Weinheim, Germany, 2016.

Supporting Information

Rust-Mediated Continuous Assembly of Metal-Phenolic Networks

*Md. Arifur Rahim, Mattias Björnmalm, Nadja Bertleff-Zieschang, Quinn Besford, Srinivas Mettu, Tomoya Suma, Matthew Faria, and Frank Caruso**

Materials. Gallic acid (GA), tannic acid (TA), pure iron (99.9%) wire, and iron(III) oxide (Fe_2O_3) pieces were purchased from Sigma-Aldrich and used as received. Commercial bright steel nails (Paslode, diameter × height: 2.8 mm × 50 mm, product number N906600) were purchased from Bunnings, Australia. Polystyrene (PS) particles (D = 3.20 ± 0.13 μm, Lot: PS/Q-R-B1229) were purchased from Microparticles GmbH. Tetrahydrofuran (THF), ethanol, and acetone were purchased from ChemSupply. High-purity (Milli-Q) water with a resistivity of 18.2 MΩ·cm was obtained from an inline Millipore RiOs/Origin water purification system.

Characterization. Differential interference contrast (DIC) microscopy images were taken with an inverted Olympus IX71 microscope. UV–Visible absorption spectra were collected on a Varian Cary 4000 UV-Vis spectrophotometer. Raman spectroscopy was performed using a Renishaw 2000 system with a Peltier cooled CCD detector, coupled to an Olympus BH-2 confocal microscope. The excitation source used with this instrument was 782 nm (NIR diode) laser lines. Laser power at the sample was 2–5 mW. The Raman signal was collected with a spectral resolution of 1 cm^{-1} over the range 100–2000 cm^{-1} using 20× or 50×

microscope objectives. For the sample preparation, concentrated capsule suspensions were cast onto Piranha cleaned boro-silica glass and dried in air. Atomic force microscopy (AFM) experiments were carried out with a JPK NanoWizard II BioAFM. Typical scans were performed in tapping mode with MikroMasch silicon cantilevers (NSC/CSC). The film thickness and roughness of the air-dried capsules were analyzed (at least 20 different capsules for each sample) using JPK SPM image processing software (version V.3.3.32). Transmission electron microscopy (TEM) images and energy dispersive X-ray spectroscopy (EDX) profiles were acquired using a FEI Tecnai TF20 instrument with an operation voltage of 200 kV. In AFM and TEM/EDX experiments, the capsule suspensions (2-10 μL) were allowed to air-dry on glass slides (Piranha cleaned) and formvar-carbon coated copper grids, respectively.

X-ray photoelectron spectroscopy (XPS) was performed on a VG ESCALAB220i-XL spectrometer equipped with a hemispherical analyzer. The incident radiation used was monochromatic Al Kα X-rays (1486.6 eV) at 220 W (22 mA and 10 kV). Survey (wide) and high-resolution (narrow) scans were recorded at analyzer pass energies of 100 and 50 eV, respectively. Survey scans were obtained using a step size of 1.0 eV and a dwell time of 100 ms. Narrow high resolution scans were run over a 20 eV binding energy range with a 0.05 eV step size and a 250 ms dwell time. The base pressure in the analysis chamber was less than 8.0×10^{-9} mbar. A low energy flood gun was used to compensate for surface charging effects. All data were processed using CasaXPS software, and the energy calibration was referenced to the C 1s peak at 285.0 eV. Solid rust powder (scrapped from a rusted nail by a sharp stainless steel blade) and dried capsule samples were used for the XPS measurements. X-ray diffraction (XRD) patterns of dried capsules (on silicon wafers), a bare silicon wafer, and powdered rust samples were collected using a Bruker D8 Advance X-ray diffractometer with Ni-filtered Cu kα radiation (1.54 Å). Data were collected between 5–90° 2θ, with a step size of 0.02°, and a scan rate of 1.0 s per step. An incident beam divergence of 1.0° was used with

a 2.5° Soller slit in the diffracted beam. The samples were spun at 15 revolutions per minute. Phase identification of the rust sample was completed using Diffrac.EVA V4.1 software with the ICDD PDF4+ 2015 database. The peaks associated with the silicon wafer were subtracted from the XRD spectrum for the capsules.

Rusting of Iron Nails. Commercial iron nails were rusted according to literature reports[1,2] with slight modifications. Briefly, 25 pieces of iron nails were degreased first by wiping with acetone-wet tissue (Kimwipe) and then sonicated in acetone for 10 min. The degreased nails were then thoroughly washed with Milli-Q water and air-dried. Next, 51 mL of 10% HCl was taken in a 250 ml glass beaker. The washed nails were placed from top of the beaker with a gap of 3.8 cm from the top surface of the HCl solution (Figure S1) and the beaker was kept in a fume hood. After 20 h, strongly adherent rust layers were observed to have formed on each nail surface and the rusted nails were removed from the beaker. After incubation in Milli-Q water for 10 min, the rusted nails were thoroughly washed with Milli-Q water and air-dried. The dried rusted nails (set A) were stored under vacuum before use. Another set of rusted nails (set B) with thicker rust layers were produced in the same manner as above except that 5% HCl and 72 h of treatment time were used in this case.

GA/R-Fe^{III} Film Formation on Particulate Substrates. GA solution (2.55 mg mL^{-1} in water, pH adjusted to 4 with 1 M NaOH) of 3 mL was taken in a 5 mL glass vial and 300 µL of PS particles (aqueous dispersion, 10%, w/w) was added under stirring (400 rpm). A rusted nail (set A, see "Rusting of Iron Nails" above) was then added to this solution from top of the vial (~3 cm of the nail was in contact with the solution) and kept stirring. 200 µL of GA/R-Fe^{III} coated PS particles were taken out from the glass vial from time to time (for standard characterization particles taken out after 1.5 or 2 h, Figure 1, main text) and processed further to obtain hollow capsules as follows: unreacted supernatant was removed by centrifugation (1700 *g*, 1 min) followed by four washing steps in Milli-Q water. Dissolution

of the PS cores was achieved by washing the coated pellet with THF four times (1900 *g*, 1 min). The obtained hollow capsules were washed twice (1700 *g*, 3 min) with Milli-Q water and finally resuspended in 100 µL of Milli-Q water for characterization. For the time-dependent thickness increase of the GA/R-Fe^{III} films, particles were taken out starting from 1.5 to 3 h with 15 min intervals and processed as above to obtain hollow capsules at each time points.

Capsules with a thickness of ~70 nm were prepared in the same manner as above except that 150 µL of PS particles and a rusted nail with thicker rust layer was used (set B, see "Rusting of Iron Nails" above) in this case. Note that, with the thicker MPN coatings, core removal became increasingly difficult and longer treatment in THF was necessary (~6 h). This also induced large pores in the films and the collapsed dried capsules appeared rougher under TEM (Figure 2g, main text). During AFM imaging it was also difficult to attain a good topographic image due to the large thickness of the capsules.

Rusted iron objects (due to natural weathering), i.e., wire, coil, drill rod, etc., were collected from various outdoor sites, washed in ethanol followed by sonication in Milli-Q water for 10 min, and air-dried. These objects were tested for GA/R-Fe^{III} coatings in the same manner as above where wire, coil or drill rod was used in place of the rusted nail. Coated particles were taken out from the reaction vial after 2-3 h and processed further as above to obtain hollow capsules.

TA/R-Fe^{III} Film Formation on Particulate Substrates. TA solution (0.25 mg mL^{-1} in water, pH adjusted to 4.5 using 1 M NaOH) of 3 mL was taken in a 5 mL glass vial and 300 µL of PS particles (aqueous dispersion, 10 wt.% solids) was added under stirring (400 rpm). A rusted nail was then added to this solution from the top of the vial (3 cm of the nail was in contact with the solution) and kept under stirring. 200 µL of TA/R-Fe^{III} coated PS particles were taken out in 1.7 mL plastic tubes over time (2, 2.5, and 3 h) and processed to

obtain hollow capsules as follows: unreacted supernatant was removed by centrifugation (1700 *g*, 1 min) followed by four washing steps in Milli-Q water. Dissolution of the PS cores was achieved by washing the coated pellet with THF four times (1900 *g*, 1 min). The obtained hollow capsules were washed twice (1700 *g*, 3 min) with Milli-Q water and finally resuspended in 100 μL of Milli-Q water for characterization.

Disassembly Experiments. GA/R-Fe^{III} capsule (~10, ~20, and ~30 nm shell thickness) suspensions (~4 × 10^7 capsules mL^{-1}) were mixed with an equal volume of disassembly solution (KCl-HCl buffer, 100 mM, pH = 2). Disassembly was monitored for each system by UV-Vis absorption spectroscopy by the decrease in the ligand to metal charge transfer (LMCT) band intensity with time. For comparison, disassembly of the conventional GA/Fe^{III} capsules (~10 nm, prepared according to our previous report)[3] was also tested in identical conditions as above.

Mechanical Tests. Details of the AFM force measurements and colloidal probe preparation can be found elsewhere.[4] Briefly, the measurements were performed on a NanoWizard II (JPK) in Milli-Q water using colloidal probe cantilevers. To fabricate the modified cantilevers, tipless cantilevers (MLCT-O, Bruker AFM Probes) were used. A spherical glass bead (D = 28.2 μm, Polysciences) was attached to the cantilever using an epoxy resin (Selleys Araldite Super Strength, Selleys) via micromanipulation employing an AFM system and associated optics. The probe was then allowed to dry overnight. Glass slides and cantilevers were cleaned with isopropanol, water, and plasma treatment to remove adventitious contamination. The modified cantilevers were first calibrated on a cleaned glass substrate to determine the inverse optical lever sensitivity (InvOLS), and the spring constant was determined to be 0.122 N m^{-1} using the thermal noise method. PEI-coated glass slides were used to immobilize the capsules prior to the measurements. Force-distance curves were obtained by optically positioning the probe over individual capsules (GA/R-Fe^{III} capsules with

~10, ~20, and ~30 nm thickness) and an approach-retract cycle with a force load of 2.5 nN and a constant piezo velocity of 1 µm s^{-1} was initiated. Force spectra of at least 10 different capsules per system were collected and analyzed using JPK data processing software. A baseline was first subtracted from the noncontact z-range of the force-displacement data and a probe/surface contact point was assigned. After subtracting the effect of the cantilever bending, force-deformation (F-δ) data were obtained. The Young's modulus (E_Y) of the spherical capsules could be estimated using the Reissner model for thin-walled spherical shells. The E_Y of GA/R-Fe^{III} capsules (~10 nm thickness) was determined using the Reissner equation with a wall thickness (h) of 10 nm, a Poisson's ratio (ν) of 0.5, and an effective probe radius (R_{eff}) of 1.61 µm. Only the deformation data over the capsule shell thickness was used.

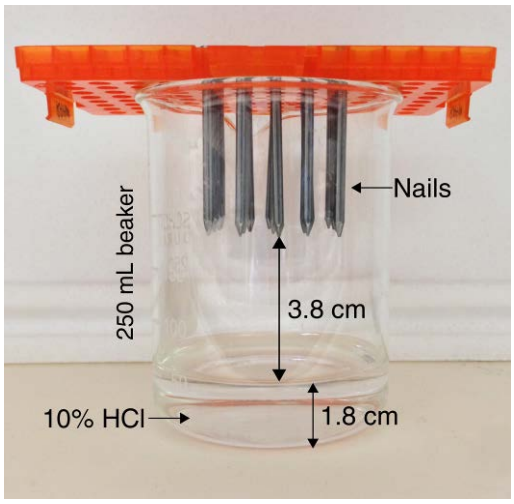

Figure S1. Set-up for the rusting process of the commercial iron nails (see "Rusting of Iron Nails" above).

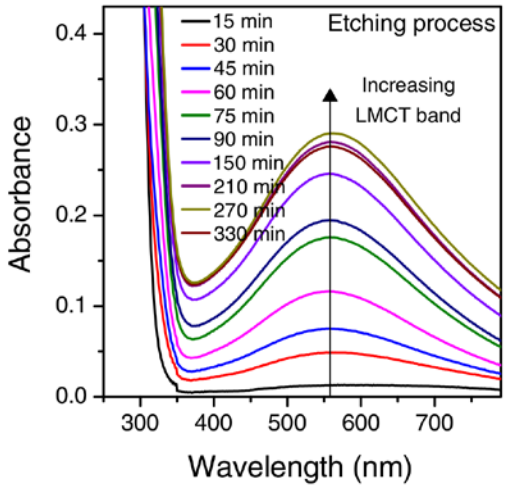

Figure S2. UV-Vis absorption spectra of the etching process over time as indicated by the increasing LMCT band intensity at ~565 nm. Absorbance values at 565 nm over time: 0.01286 (15 min), 0.04857 (30 min), 0.07476 (45 min), 0.11569 (60 min), 0.17509 (75 min), 0.19398 (90 min), 0.24487 (150 min), 0.28028 (210 min), 0.29019 (270 min), and 0.27525 (330 min).

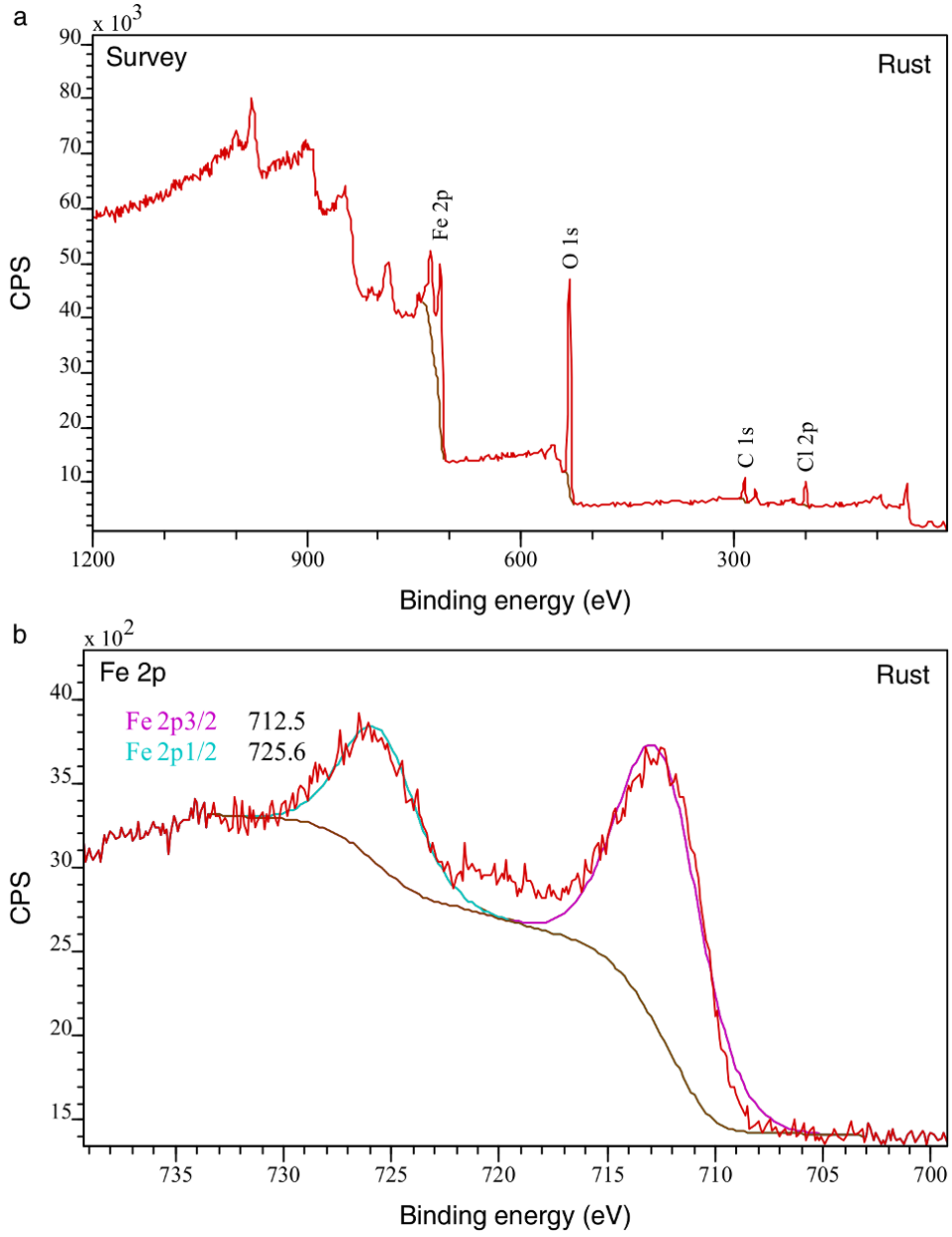

Figure S3. XPS spectra showing the composition of rust. Survey spectrum (a) detected carbon that is in agreement with the mild steel composition. The chlorine signal may originate from the residual chlorine during the rusting process in HCl vapor (see "Rusting of Iron Nails"). Fe 2p core-level spectrum (b) confirmed the oxidation state of III for Fe.[5]

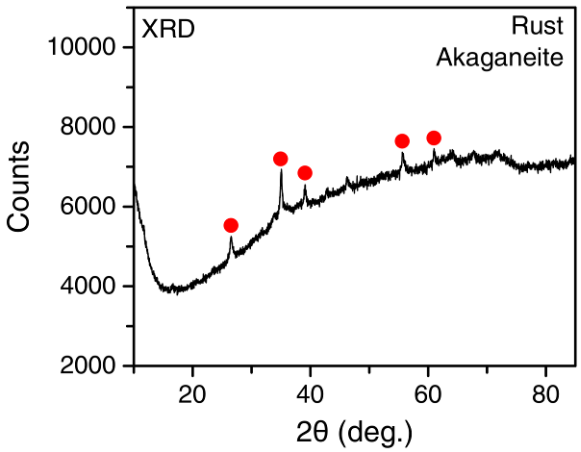

Figure S4. XRD characterization of the rust. Peaks were identified (indicated by red dots) at 26.535°, 35.075°, 39.101°, 55.686°, and 61.037°. This crystalline phase was identified as akaganeite (β-FeO(OH)), International Centre for Diffraction Data (ICDD) PDF database number: 00-060-0614.

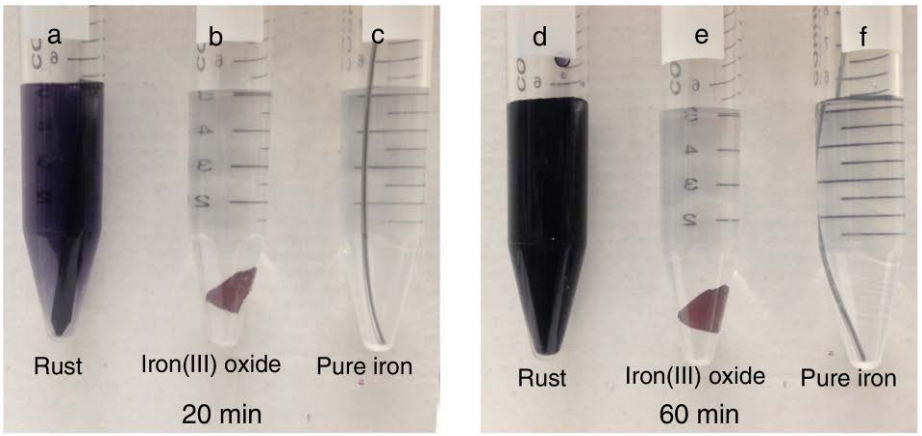

Figure S5. Photographs of the etching tests performed for iron(III) oxide (Fe_2O_3) (b, e) and pure iron (c, f) in GA solution (2.55 mg mL^{-1}, pH ~4) after 20 and 60 min, respectively, and no etched GA/Fe^{III} complexes (blue-black color) were observed in these cases. In comparison, a rusted iron nail produced the blue-black GA/Fe^{III} complexes via etching (a, d).

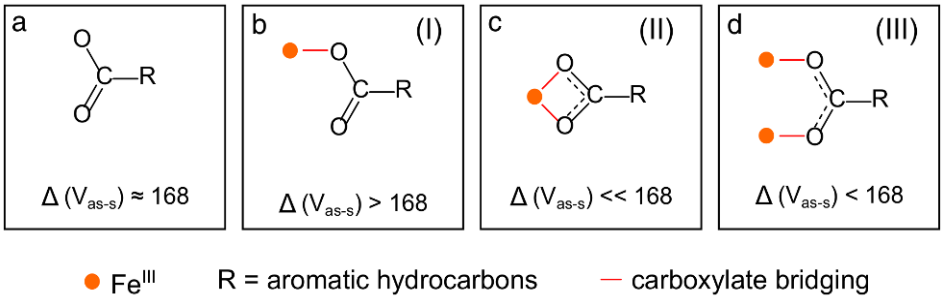

Figure S6. Assignments of the different types (I-III) of coordination modes (a-d) of the -COO group of GA with Fe^{III}. These assignments are based on the difference between symmetric and asymmetric stretching vibrations of -COO group.[6]

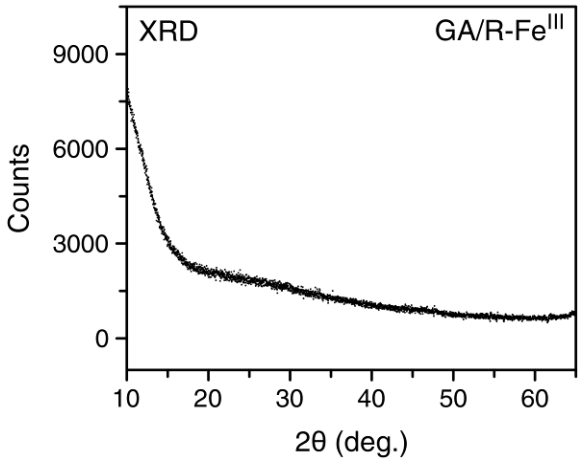

Figure S7. XRD characterization of the dried GA/R-Fe^{III} capsules suggesting an amorphous phase of the system.

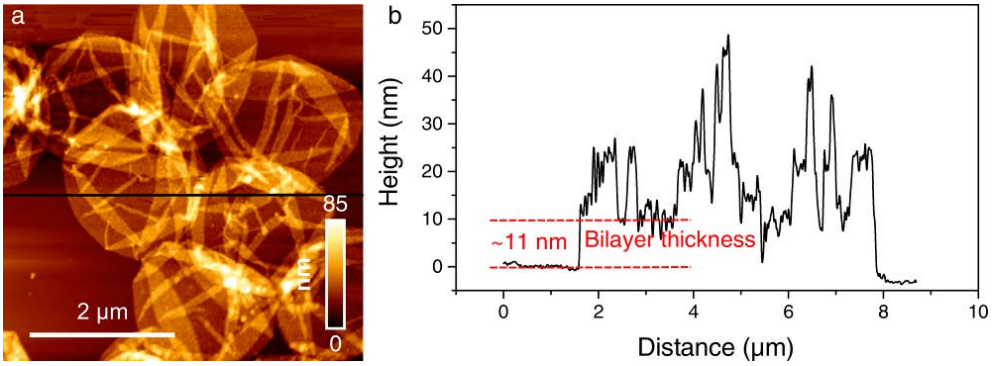

Figure S8. AFM micrograph (a) of the GA/R-Fe^{III} capsules (obtained after 1.5 h from the immersion of the rusted iron nail in GA solution) and the corresponding height profile (b) showing the collapsed bilayer thickness of the films (capsule shell thickness can be calculated as half of the bilayer thickness).

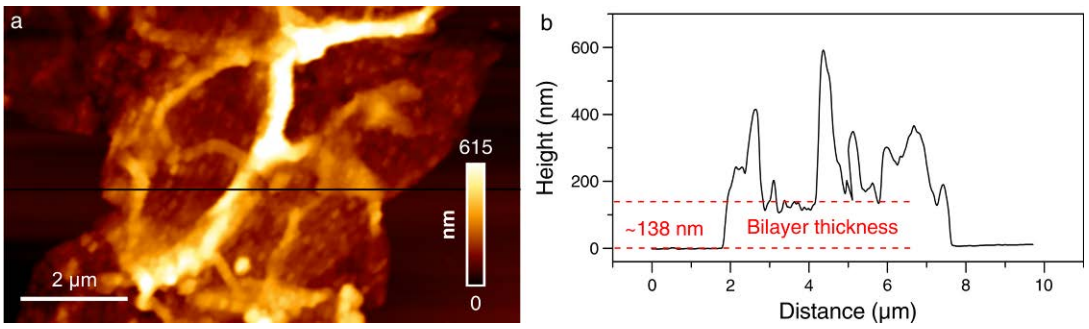

Figure S9. AFM micrograph (a) of the GA/R-Fe^{III} capsules obtained using a thicker rust layer and lower concentration of PS particles (see "GA/R-Fe^{III} Film Formation on Particulate Substrates" for details), and the corresponding height profile (b) showing the collapsed bilayer thickness of the films (capsule shell thickness can be calculated as half of the bilayer thickness, i.e., ~70 nm in this case).

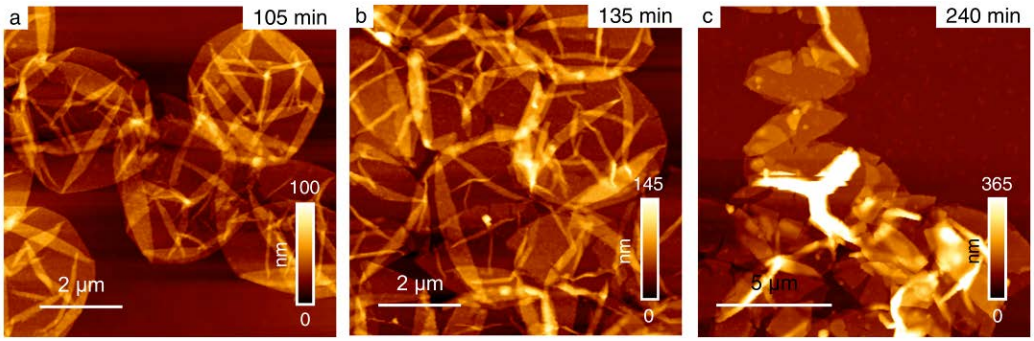

Figure S10. AFM topographic images (a-c) of the GA/R-Fe^{III} capsules with increasing thickness over time.

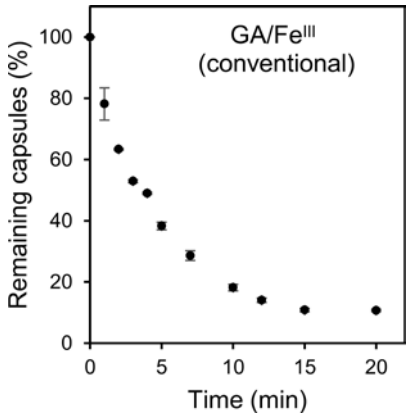

Figure S11. Disassembly profiles of the GA/Fe^{III} capsules (shell thickness of ~10 nm) prepared by the conventional bulk solution assembly.

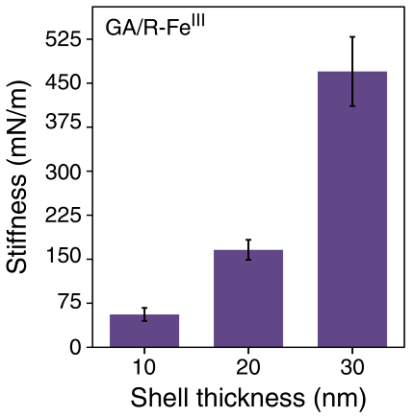

Figure S12. Stiffness of the GA/R-Fe^{III} capsules with increasing shell thickness as determined by colloidal-probe AFM measurements.

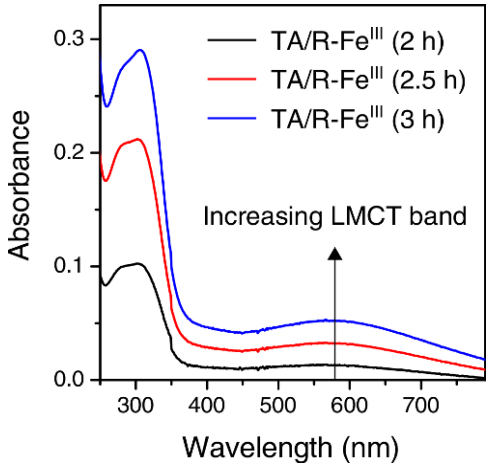

Figure S13. UV-Vis absorption spectra of the TA/R-Fe^{III} capsules obtained over time from the immersion of a rusted nail in TA solution, showing the continuous assembly process for this system.

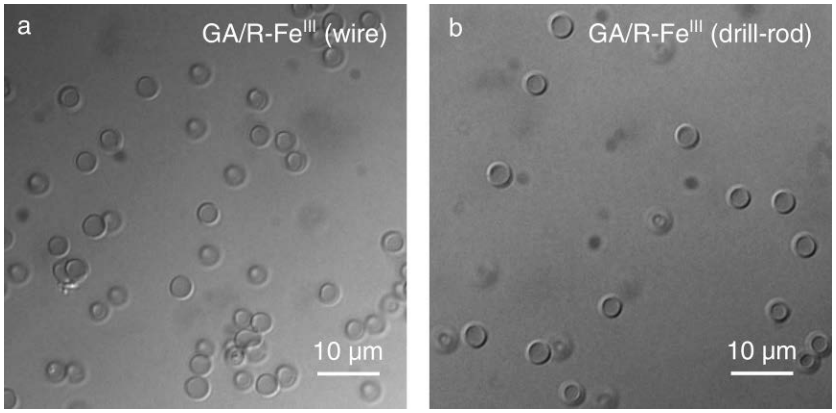

Figure S14. DIC images of the GA/R-Fe^{III} capsule dispersions obtained using the collected rusted wire (a) and drill-rod (b), showing stable and monodisperse capsules.

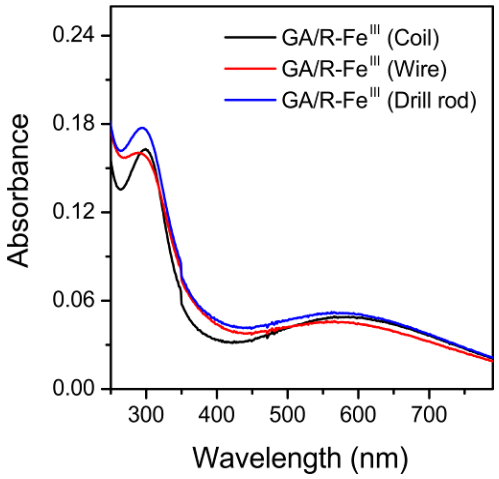

Figure S15. UV-Vis absorption spectra of the GA/R-Fe^{III} capsules obtained using the collected rusted coil, wire, and drill-rod. LMCT bands for these samples appeared around 570 nm.

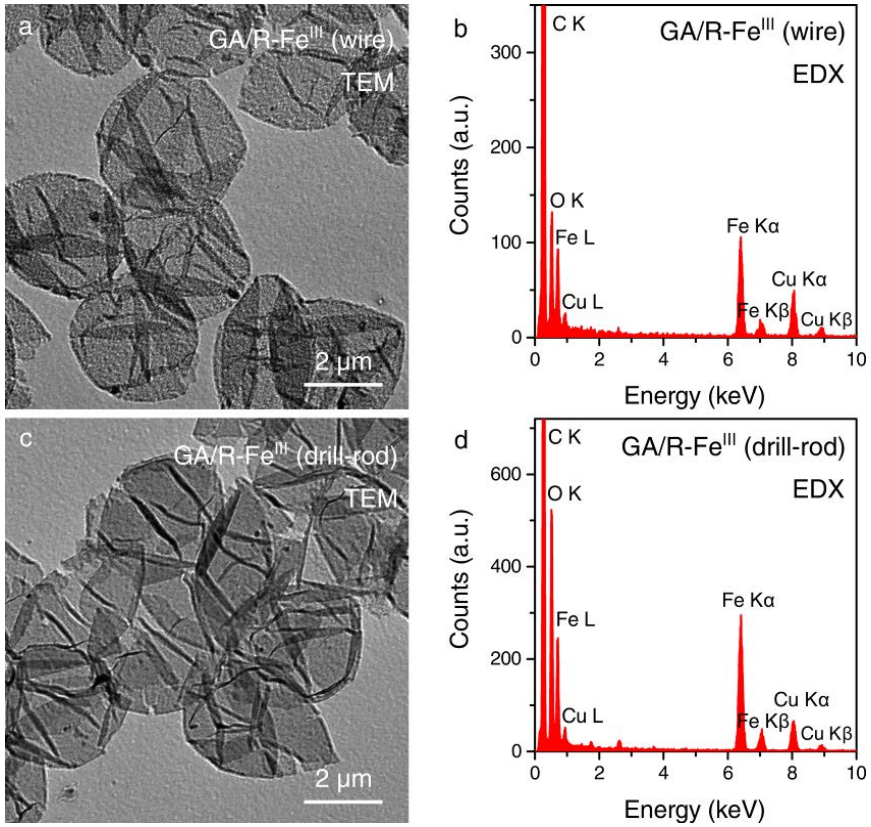

Figure S16. TEM micrographs of the GA/R-Fe^{III} capsules obtained using the collected rusted wire (a) and drill-rod (c). EDX analyses (b, d) of the corresponding systems showing the presence of iron.

Supporting References

[1] S. C. Okoro, M. Montgomery, F. J. Frandsen, K. Pantleon, *Energy Fuels* **2015**, *29*, 5802.

[2] R. Pietrzak, R. Szatanik, *Phys. Status Solidi* **2010**, *247*, 1822.

[3] M. A. Rahim, K. Kempe, M. Müllner, H. Ejima, Y. Ju, M. P. van Koeverden, T. Suma, J. A. Braunger, M. G. Leeming, B. F. Abrahams, F. Caruso, *Chem. Mater.* **2015**, *27*, 5825.

[4] M. A. Rahim, H. Ejima, K. L. Cho, K. Kempe, M. Müllner, J. P. Best, F. Caruso, *Chem. Mater.* **2014**, *26*, 1645.

[5] J. F. Moulder, J. Chastain, *Handbook of X-ray Photoelectron Spectroscopy: A Reference Book of Standard Spectra for Identification and Interpretation of XPS Data*, Physical Electronics Division, Perkin-Elmer Corporation, **1992**.

[6] K. Nakamoto, *Infrared and Raman Spectra of Inorganic and Coordination Compounds: Part B: Applications in Coordination, Organometallic, and Bioinorganic Chemistry*, John Wiley & Sons, Hoboken, NJ, USA **2009**.

University Library

MINERVA ACCESS

A gateway to Melbourne's research publications

Minerva Access is the Institutional Repository of The University of Melbourne

Author/s:
Rahim, MA; Bjoernmalm, M; Bertleff-Zieschang, N; Besford, Q; Mettu, S; Suma, T; Faria, M; Caruso, F

Title:
Rust-Mediated Continuous Assembly of Metal-Phenolic Networks

Date:
2017-06-13

Citation:
Rahim, M. A., Bjoernmalm, M., Bertleff-Zieschang, N., Besford, Q., Mettu, S., Suma, T., Faria, M. & Caruso, F. (2017). Rust-Mediated Continuous Assembly of Metal-Phenolic Networks. ADVANCED MATERIALS, 29 (22), https://doi.org/10.1002/adma.201606717.

Persistent Link:
http://hdl.handle.net/11343/129441

File Description:
Accepted version

License:
Publisher's own licence